International Journal of Hydrogen Energy 51 (2024) 1518–1526

Contents lists available at ScienceDirect

International Journal of Hydrogen Energy

journal homepage: www.elsevier.com/locate/he

Feasible domain of cycling operating conditions and model parameters for Holby–Morgan model of platinum catalyst degradation in PEMFC

Victor A. Kovtunenko *

Department of Mathematics and Scientific Computing, Karl-Franzens University of Graz, NAWI Graz, Heinrichstr. 36, 8010 Graz, Austria
Lavrentyev Institute of Hydrodynamics, Siberian Division of the Russian Academy of Sciences, 630090 Novosibirsk, Russia

ARTICLE INFO

MSC:
78A57
80A30
80A32
35K57

Keywords:
Proton-exchange membrane fuel cell
Catalyst degradation
Platinum dissolution and oxidation
Accelerated stress test
Sensitivity analysis
Feasible region

ABSTRACT

In the paper, electrochemical behavior of platinum based cathode catalyst in a polymer electrolyte membrane fuel cell is studied under non-symmetric square-wave electric potential cycling applied in accelerated stress test. Following the modeling by Holby and Morgan, degradation due to Pt dissolution, ion diffusion, and oxide coverage is performed with respect to cycling operating conditions and model parameters. The computer simulation demonstrates impact of the electrochemical surface area loss rate under variation of the temperature, pH, platinum particle diameter, loading, Pt to Carbon volume fraction, and their simultaneous effect. From physical consistency and multi-parametric sensitivity analysis, a statement on feasible domain of the parameters for the PEMFC operation is concluded.

1. Introduction

As a matter of principle of hydrogen storage technologies, fuel cells convert chemical energy stored in H_2 into electricity. Proton Exchange Membrane Fuel Cells (PEMFC) are especially attractive because of high power density, compactness, and low operating temperature. We refer to compendium of hydrogen energy by Ball et al. [1], Barbir et al. [2], Basile et al. [3], Subramani et al. [4], and to novel functional materials by Medvedev [5]. Compared to conventional energy development based mostly on internal combustion engines using fossil fuels, hydrogen is considered to have lower environmental problems. It has the potential of lowering CO_2 emissions, especially from heavy duty vehicles like trucks, trains, and marine vessels, as well as stationary power systems, see a life cycle assessment (LCA) by Evangelisti et al. [6], Ferrara et al. [7], Gallo and M. Marinelli [8]. In hydrogen and hybrid electric vehicles, the fuel-cell is subjected to potential oscillation that causes degradation processes of PEMFC components. Accelerated Stress Test (AST) on fuel cell catalysts confirms that during electric potential cycling degradation phenomena shorten the operating lifetime and lead to higher hydrogen consumption, see Petrone et al. [9], Macauley et al. [10]. Especially the Membrane Electrode Assembly (MEA) is responsible for performance degradation, in particular, platinum catalyst degradation. Platinum is commonly used as an electrocatalyst for the Oxygen Reduction Reaction (ORR) and belongs to critical raw materials, which have high environmental impact during its extraction, and high price because of scarcity and difficulty of replacement.

Some phenomena of PEMFC degradation were included into the environmental evaluation by Stropnik et al. [11]. In particular, a reduction of the expensive platinum content in PEMFC was reported, when Pt particle loading (the mass of particles per volume) in catalyst was reduced. On the contrary, reduction of the Pt loading leads to higher loss in electrochemical surface area, thus shortens the operating lifetime. The other phenomenon concerns size of platinum particles. Since Pt is dispersed in the form of nanoparticles on a carbon support (Pt/C), reducing the particle size improves utilization, that is the available surface area relative to mass, which itself minimizes O_2 mass transport loss necessary for high power performance. However, Pt particles of small size are thermodynamically unstable and cause catalyst degradation. These conflicting issues challenge designers and engineers and motivate fundamental investigations and numerical simulations of the problem.

Development of efficient mitigation strategies and understanding of fundamental degradation mechanisms, as well as its correlation with operating conditions, motivates mathematical modeling of platinum-based carbon-supported catalysts in PEMFC. We refer to the theoretical studies by Eikerling and Kulikovsky [12,13], Hacker and Mitsushima [14], relevant electrokinetic modeling with Butler–Volmer

* Correspondence to: Department of Mathematics and Scientific Computing, Karl-Franzens University of Graz, NAWI Graz, Heinrichstr. 36, 8010 Graz, Austria.
E-mail address: victor.kovtunenko@uni-graz.at.

https://doi.org/10.1016/j.ijhydene.2023.11.182
Received 5 May 2023; Received in revised form 25 September 2023; Accepted 15 November 2023
Available online 20 November 2023

equations in [15], Poisson–Nernst–Planck equations in [16–18], mechanical degradation and its testing in [19,20]. Karpenko–Jereb et al. [21] considered coupling degradation components in membrane of non-uniform thickness with 3D Computational Fluid Dynamics (CFD) model in Gas Diffusion Layer (GDL). Kulikovsky [22] was considered degradation due to Carbon Corrosion (CC) reaction

$$C + H_2O \leftrightharpoons CO_2 + 2H^+ + 2e^-$$

which is relatively slow process and accelerates at a potential hold of about 1.2 V. A diffusive model for carbon corrosion phenomenon was proposed by Pandy et al. [23] addressing complex interaction between the formation of oxide groups and the accumulation on carbon and Pt surfaces. In Kravos et al. [24], further performance and degradation model was calibrated on Low-Temperature (LT) PEMFC and adapted with a mechanism of carbon corrosion capable using in High-Temperature (HT) fuel cells.

Membrane degradation under fuel cell operating conditions is generally mixed due to combination of chemical, mechanical, and thermal stressors. Comprehensive overview of chemical degradation can be found in Frühwirt et al. [25]. The chemical degradation is dominated by attack of radical species formed during FC operation. Under typical operation conditions oxygen is reduced at the cathode in the ORR via different reactions, and it can diffuse to the anode side. Therefore, sufficient amount of platinum needs to be used at the cathode side to efficiently catalyze the oxygen reduction.

Electrochemical degradation dominates when applying Open Circuit Voltage (OCV) AST. Under the electric potential difference, Pt becomes electrochemically unstable, and its dissolution may start. Platinum ions Pt^{2+} dissolved into the electrolyte can diffuse in the Catalyst Layer (CL), or re-deposit through CL, as well as migrate into the membrane. The change of Pt distribution is considered as the main driver for catalyst degradation. Cherevko et al. [26] gives an overview of the literature on platinum dissolution as a constituent part of degradation mechanisms in the fuel cell electrocatalyst.

In our study we consider the platinum degradation model introduced by Holby and Morgan [27]. Originally, based on Butler–Volmer equations, Darling and Meyers [28] developed kinetic rate equations for platinum electrochemical dissolution reaction

$$Pt \leftrightharpoons Pt^{2+} + 2e^- \tag{1}$$

platinum oxide (PtO) film formation reaction

$$Pt + H_2O \leftrightharpoons PtO + 2H^+ + 2e^- \tag{2}$$

and chemical dissolution reaction

$$PtO + 2H^+ \leftrightharpoons Pt^{2+} + H_2O \tag{3}$$

Holby and Morgan refined the model by taking into account diffusion of building Pt ions into the ionomer membrane within the Pt dissolution and oxidation that is responsible for degradation, and neglected the chemical dissolution of PtO reaction (3) when compared with the major electrochemical mechanism. Li et al. [29] introduced particle size groups to represent a discrete Particle Size Distribution (PSD). Zheng et al. [30] incorporated simulation of a three-layer gradient cathode CL.

From the Holby–Morgan model it is possible to determine the relative amount of mass lost from the PSD and the particle size growth. Bi et al. [31] extended the dissolution (1) with precipitation of Pt ions by hydrogen reduction

$$Pt^{2+} + H_2 \leftrightharpoons Pt + 2H^+$$

For modeling of another degradation mechanisms: Pt ions re-deposition on neighbor particles that leads to growth of the particle size, also known as Ostwald ripening, platinum migration within the membrane that causes formation of Pt band without changing particle sizes, and its coupling with the cell model we refer the interested readers to Jahnke et al. [32], Kregar et al. [33].

Lifetime of a fuel cell is determined as the time required the cell voltage to reach some critical threshold (typically 90%) of Beginning of Life (BoL) cell voltage. The voltage is commonly called the electric potential difference versus a reference of 0 V. State of the art tests take about 30,000 operating hours for steady state, and may take from tens to thousands of hours carried out for dynamic operating of PEMFC, see a review of testing procedures for electrolyzer degradation in Tomić et al. [34]. The lack of standardization of industrial tests and accelerated protocols is especially emphasized in the review. In simulation of real operating conditions without reaching failure, reduction within the range of 10% of BoL is often considered as End of Life (EoL). At the end of our numerical tests we reach 0.4–4% level of degradation.

For a physical description of the degradation process, results by fitting experimental data to various theoretical models are typically reported in the literature. As a consequence, fitted material parameters cannot be applied to different materials. Considering involved electrochemical reactions in catalyst, common drawback is that operating conditions vary from study to study. Publicly available supplier data usually consist of only few averaged parameters like platinum particle size, Pt loading on the carbon support, and Pt/C weight ratio, which we take for testing in our consideration. To analyze significance of model parameters with respect to available experimental data, an optimization approach based on minimization of a residual error between simulated and measured data is commonly used. To attain numerically the identification of multiple input–output parameters for a nonlinear model, the local analytical linearization suggested by Ritzberger et al. [35] might be helpful.

For validation and calibration of theoretical or numerical models with experimental data, the method of sensitivity analysis is useful, see Correa et al. [36], Min et al. [37], Pant et al. [38]. The parameter sensitivity means how variation of input parameters impacts performance or durability of PEMFC operation via representative outputs. It allows to determine the relative importance of each parameter on the model result. The sensitivity analysis is typically conducted individually by varying one parameter at a time (OAT method), maintaining remaining parameters at values of the basic case. In the case of linear dependence, linear regression based on covariance is a reasonable tool. However, we deal with the Butler–Volmer equation, which is of exponential type, hence highly nonlinear. One parameter may have a positive effect increasing performance, while another may have a negative effect, thus giving raise to multi-parametric analysis. The simultaneous effect when multiple parameters are varied together is much more involved technically and scarcely reported in the literature.

The range is a measure of variation, which prescribes upper and lower limits for the parameter variation based on physical consistency. For instance, many of physical parameters such as temperature, radius, concentration, and alike should be non-negative. Fractional parameters typically have minimal and maximal thresholds like 0 and 1. The other critical values may arise when attaining infeasible PEMFC operation at which the fuel cell or its component does not work anymore. Such critical values build a feasible region for variation of test parameters. Identifying the feasible domain for operating conditions, model parameters, and their interplay is our current task, which helps to focus future mitigation strategies. In order to quantify the result of sensitivity analysis, in the present paper we take the electrochemical surface area loss rate as the output of catalyst degradation.

2. Model and methods

The Holby–Morgan model accounts for three mechanisms of catalyst degradation, namely: platinum dissolution according to the electrochemical reaction (1), platinum oxidation according to the electrochemical reaction (2), and platinum ion diffusion in the membrane. This includes the effects of particle size distribution, interfacial thermodynamics, and hydrogen crossover from the anode to the cathode. The model is one dimensional along the direction normal to the cathode

Table 1
Parameters for Pt ion formation and diffusion, and Pt oxide formation.

Symbol	Value	Units	Description
ν_1	1×10^4	Hz	dissolution attempt frequency
ν_2	8×10^5	Hz	backward dissolution rate factor
β_1	0.5		Butler transfer coefficient for Pt dissolution
n	2		electrons transferred during Pt dissolution
$U_{\rm eq}$	1.118	V	Pt dissolution bulk equilibrium voltage
Ω	9.09	$\rm cm^3/mol$	molar volume of Pt
γ	2.4×10^{-4}	$\rm J/cm^2$	Pt [1 1 1] surface tension
$c_{\rm ref}$	1	$\rm mol/cm^3$	reference Pt ion concentration
$H_{1,\rm fit}$	4.4×10^4	J/mol	partial molar Pt dissolution activation enthalpy
$D_{\rm Pt}$	1×10^{-6}	$\rm cm^2/s$	diffusion coefficient of Pt ion in the membrane
$\nu_1^\star$	1×10^4	Hz	forward Pt oxide formation rate constant
$\nu_2^\star$	2×10^{-2}	Hz	backward Pt oxide formation rate constant
Γ	2.2×10^{-9}	$\rm mol/cm^2$	Pt surface site density
β_2	0.5		Butler transfer coefficient for PtO formation
n_2	2		electrons transferred during Pt oxide formation
$U_{\rm fit}$	0.8	V	Pt oxide formation bulk equilibrium voltage
λ	2×10^4	J/mol	Pt oxide dependent kinetic barrier constant
ω	5×10^4	J/mol	Pt oxide-oxide interaction energy
$H_{2,\rm fit}$	1.2×10^4	J/mol	partial molar oxide formation activation enthalpy

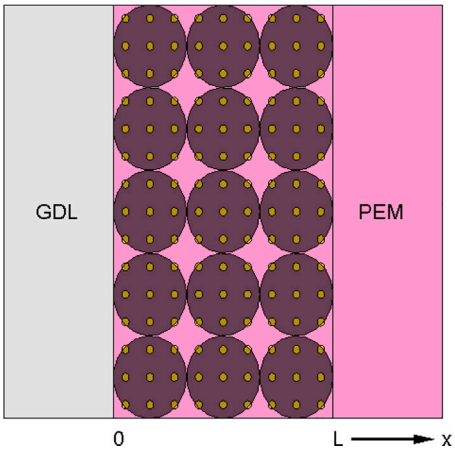

Fig. 1. GDL–CL–PEM cross section.

and mean-field in the plane orthogonal to this direction. Indeed, the thickness of MEA is much smaller than its in-plane dimensions, and Pt particles are assumed to be uniformly distributed. More discussion of the modeling issues can be found in [39] and references therein.

In Table 1 we gather physical parameters for platinum ion formation and diffusion, and for platinum oxide formation, which are taken from the literature [23,27–29] for the further use in computer simulation.

2.1. Nonlinear reaction–diffusion equations

Let us consider the catalyst layer of thickness $L = 10$ μm, and the 1D variable $x \in [0, L]$ such that the CL matches GDL at the left end $x = 0$, and PEM at the right end $x = L$, as illustrated in Fig. 1 For $x \in (0, L)$ and prescribed voltage $V(t)$ in time $t > 0$, we look for unknown platinum ion concentration $c(t, x)$ written in $\rm mol/cm^3$, platinum particle diameter $d(t, x)$ in cm, and dimensionless platinum oxide coverage ratio $\theta(t, x)$ satisfying the coupled system of nonlinear reaction–diffusion equations according to [29]:

$$\varepsilon\frac{\partial c}{\partial t} - \varepsilon^{3/2}D_{\rm Pt}\frac{\partial^2 c}{\partial x^2} = \frac{\pi N}{2}d^2 r_{\rm dissol}(c,d,\theta) \tag{4}$$

$$\frac{\partial d}{\partial t} = -\Omega\, r_{\rm dissol}(c,d,\theta) \tag{5}$$

$$\frac{\partial \theta}{\partial t} + 2\theta\frac{\partial(\ln d)}{\partial t} = \frac{1}{\Gamma}r_{\rm oxide}(\theta) \tag{6}$$

where N is the number concentration of Pt particles in the CL. The reaction rates $r_{\rm dissol}$ and $r_{\rm oxide}$ in (4)–(6) are given according to a Butler–Volmer equation and measured in $\rm mol/(cm^2\,s)$. The Pt ion dissolution (1) is described by

$$r_{\rm dissol}(c,d,\theta) = \Gamma(1-\theta)\exp\Big\{-\frac{H_{1,\rm fit}}{RT}\Big\} \times\Big(\nu_1\exp\Big\{-\frac{1-\beta_1}{RT}H_1(d,\theta)\Big\} - \frac{\nu_2 c}{c_{\rm ref}}\exp\Big\{\frac{\beta_1}{RT}H_1(d,\theta)\Big\}\Big) \tag{7}$$

using the partial molar enthalpy difference for dissolution [J/mol]

$$H_1(d,\theta) = nF(U_{\rm eq}-V) - \frac{4\Omega}{d}\big(\gamma_0(\theta) - \Gamma n_2 F\theta V\big) \tag{8}$$

where F is the Faraday constant, R is the gas constant, and the surface tension difference

$$\gamma_0(\theta) = \gamma + \Gamma RT\theta\Big(\ln\Big(\frac{\nu_2^\star}{\nu_1^\star}10^{-2pH}\Big) + \frac{2n_2FU_{\rm fit}+\omega\theta}{2RT} + \ln\Big(\frac{\theta}{2}\Big) + \frac{2-\theta}{\theta}\ln\Big(1-\frac{\theta}{2}\Big)\Big) \tag{9}$$

is given in $\rm J/cm^2$. The Pt oxide coverage (2) is described by

$$r_{\rm oxide}(\theta) = \Gamma\exp\Big\{-\frac{H_{2,\rm fit}+\lambda\theta}{RT}\Big\} \times\Big(\nu_1^\star\Big(1-\frac{\theta}{2}\Big)\exp\Big\{-\frac{1-\beta_2}{RT}H_2(\theta)\Big\} - \nu_2^\star 10^{-2pH}\exp\Big\{\frac{\beta_2}{RT}H_2(\theta)\Big\}\Big) \tag{10}$$

using the partial molar enthalpy difference for oxidation [J/mol]

$$H_2(\theta) = n_2F(U_{\rm fit}-V) + \omega\theta \tag{11}$$

The system of Eqs. (4)–(11) is endowed with the initial condition for $x \in [0, L]$:

$$c(0,x) = 0, \quad d(0,x) = d_{\rm Pt}, \quad \theta(0,x) = 0 \tag{12}$$

for prescribed $d_{\rm Pt}$, the no-flux condition at the GDL–CL interface for $t > 0$:

$$\frac{\partial c}{\partial x}(t,0) = 0 \tag{13}$$

and zero concentration of dissolved ions at the CL–PEM interface for $t > 0$:

$$c(t,L) = 0 \tag{14}$$

The physical consistency implies positive concentration

$$c(t,x) > 0 \tag{15}$$

positive particle diameter

$$d(t,x) > 0 \tag{16}$$

also minimum and maximum values for ratio

$$0 < \theta(t,x) < 1 \tag{17}$$

The constraints (15)–(17) form feasible region for solutions of Eqs. (4)–(14). The feasibility of solution may in turn cause restriction on variation of operating conditions and parameters involved in the model. The domain of feasible parameters is the subject of our investigation in the context of platinum catalyst degradation.

2.2. Electro chemical surface area loss rate

To quantify platinum degradation under cycling operating conditions, performance of Electro Chemical Surface Area (ECSA) is commonly reported in the literature. The ECSA is a key parameter of fuel cell electrodes since increasing surface area increases rate of reaction. The amount of ECSA can be determined by the following formula [27]:

$$\mathrm{ESCA} = 0.63\,\frac{\pi N}{2} d^2 \tag{18}$$

assuming hemispherical Pt particles of diameter d, where N represents the number of particles at a reference diameter, and 0.63 can be taken for an average value of ECSA/GSA ratio from experiments. Within small and moderate times T_{EoL}, a close to linear decay takes place. During long-time tests, in experiments was observed that the most loss of ECSA happens in the beginning of potential cycles.

We apply the European Union recommended Fuel Cell and Hydrogen Joint Undertaking (FCH 2JU) AST protocol [40] by non-symmetric Square-Wave (SW) between the lower potential $V(t) = 0.6$ V during $t = 10$ s, and the upper potential $V(t) = 0.9$ V during $t = 30$ s at each cycle. For numerical solution of the nonlinear reaction–diffusion Eqs. (4)–(14) under the cycling $V(t)$ we apply an implicit-explicit scheme together with variable time-step Runge–Kutta method, where a step-size is refined locally at the electric potential lift-off, as presented in details in Ref. [41]. The source code is written using standard MATLAB routines. For illustration, in Fig. 2 we plot a simulated by the Holby–Morgan model evolution of ECSA ratio E, which is computed according to (18) as

$$E(t) = \Big(\frac{d(t)}{d_{\mathrm{Pt}}}\Big)^2, \quad E(0) = 1 \tag{19}$$

when the particle diameter $d(t)$ decreases from an initial value $d(0) = d_{\mathrm{Pt}}$ due to platinum degradation. In plot (a) the dimensionless function $E(t)$ from (19) is depicted versus time $t \in (0, T_{\mathrm{EoL}})$ in hour scale. Whereas in plot (b) this curve is zoomed in minute scale and performs typical waves under potential cycles. From Fig. 2(a) we evaluate initial loss of ECSA about 0.37% per hour during simulation $T_{\mathrm{EoL}} = 11$ h (1000 cycles). In plot (c) the ECSA loss rate is compared when computed at the end of 10, 100, and 1000 cycles: it slightly decays with the number of cycles. In experiments of Pivac and Barbir [42], the change of electrochemical surface area by the AST was quantified applying cyclic voltammetry, where the ECSA loss rate in the range of 0.19–0.4% per hour was recorded during the longer operating time $T_{\mathrm{EoL}} = 27.5$ h (2500 cycles) shown by the error bar in the plot (a) of Fig. 2. This comparison was done for calibration of the fitting parameters from Table 1.

Based on the simulation tests we conclude that, for a qualitative analysis within reasonable times T_{EoL} we can approximate the ECSA ratio by an affine function

$$E(t) \approx 1 - t\dot{E} \quad \text{for } t \in (0, T_{\mathrm{EoL}}), \tag{20}$$

with a time-independent rate $\dot{E} > 0$. To avoid any confusion, ESCA does not in general follow linear trend. The specific form of ESCA time profile depends strongly on the underlying mechanism of particle growth, as explained in Kregar et al. [43]. In our further consideration we will take the averaged initial rate $\dot{E}$ of ECSA ratio loss according to the approximation (20):

$$\dot{E} := \frac{1 - E(T_{\mathrm{EoL}})}{T_{\mathrm{EoL}}} \tag{21}$$

as a natural output parameter measuring platinum catalyst degradation in PEMFC in the beginning of potential cycles when varying operating conditions and model parameters.

3. Results and discussion

In our previous works by Karpenko–Jereb and Kovtunenko [39,41] we studied the Holby–Morgan model for different industrial protocols with respect to triangle and square shaped voltage profiles, their upper potential level (UPL) and lower potential level (LPL), respective dwell times. The loss of Pt mass and respective active area drops at low humidity (water activity), operational temperature, dwell time at UPL. The dissolution process at low potential is accelerated at high temperature in PEMFC and with a decrease in pH value.

In the current work we investigate cycling operating conditions of temperature $T > 0$ and pH ≥ 0, model parameters of Pt particle diameter $d_{\mathrm{Pt}} \geq 0$, Pt particle loading $p_{\mathrm{Pt}} \geq 0$, and Pt to Carbon (Pt/C) volume fraction $\varepsilon \in (0, 1]$ with respect to their feasible values, and the simultaneous effect. As the reference values we set $T = 353.15$ K corresponding to 80 °C, pH = 0, $d_{\mathrm{Pt}} = 3$ nm, $p_{\mathrm{Pt}} = 0.4$ mg/cm^2, and $\varepsilon = 0.2$.

3.1. Sensitivity to temperature operating condition

In automotive applications, a fuel cell is expected to perform under a wide range of operating conditions, including the temperature range from −40 °C to 100 °C. Whereas LT-PEMFC operates up to about 90 °C, HT-PEMFC functions up to 180 °C. In the both LT and HT cases, the catalyst material is similarly made of fine Pt nanoparticles dispersed over a highly porous matrix of carbon black providing good transport properties and high electric conductivity. Operation at higher temperatures allows for better heat rejection, however, in previous studies there was reported accelerated cathode catalyst degradation in this case. Cathodic dissolution prevails over anodic dissolution with respect to the overall amount of dissolved Pt and depends strongly on the pH.

Zhao et al. [44] concluded that lifetime of MEA increases with decreasing cell temperature trends from high 95 °C to moderate 64 °C, as predicted by transport phenomena. In Kregar et al. [33], physically based degradation model was calibrated by fitting the results of experimental measurements in Maselj et al. [45] for changes in ECSA during Triangle-Wave (TW) electric potential AST performed on catalyst layer. The experiments were performed for various potential cycle protocols and low temperatures in the range from 20 °C to 60 °C. The following features were reported: The degradation of the catalyst and the consequent loss of ESA is mostly caused by the dissolution of small Pt particles and the re-deposition of Pt ions on larger particles increasing the mean particle size. Compared to the main dissolution mechanism, carbon corrosion plays minor role in particle growth at temperatures below 60 °C. The increase in degradation rate at higher temperatures is attributed to the Arrhenius equation for temperature-dependent parameters in reaction rates.

In Fig. 3 we present our result of numerical simulation by the Holby–Morgan model. The values of the ECSA ratio loss rate $\dot{E}$ are computed during $T_{\mathrm{EoL}} = 1.1$ h (100 cycles) according to Eq. (21) when varying the temperature T from 10 °C to 120 °C, and pH from 0 to 4. The $\dot{E}$-curves are depicted with respect to increasing T at selected

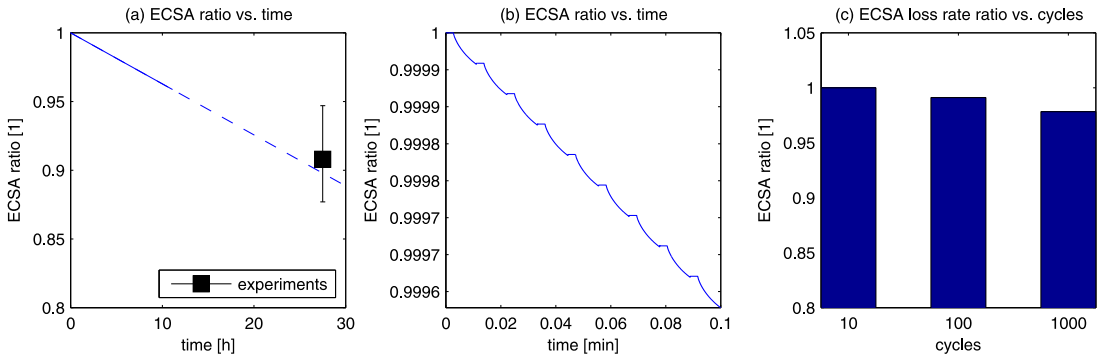

Fig. 2. Example $E(t)$ evolution in hour scale (a), its zoom in minute scale (b), and presented in diagram with respect to the number of cycles (c).

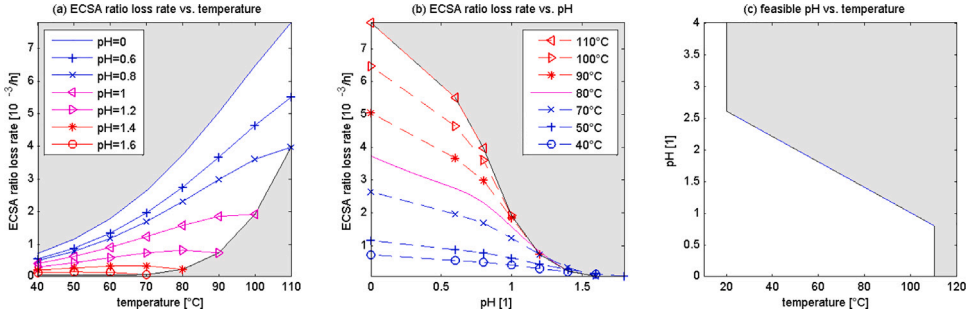

Fig. 3. ECSA ratio loss rate $\dot{E}$ depending on temperature T for various pH (a), $\dot{E}$ depending on pH for various T (b), feasible domain pH–T (c).

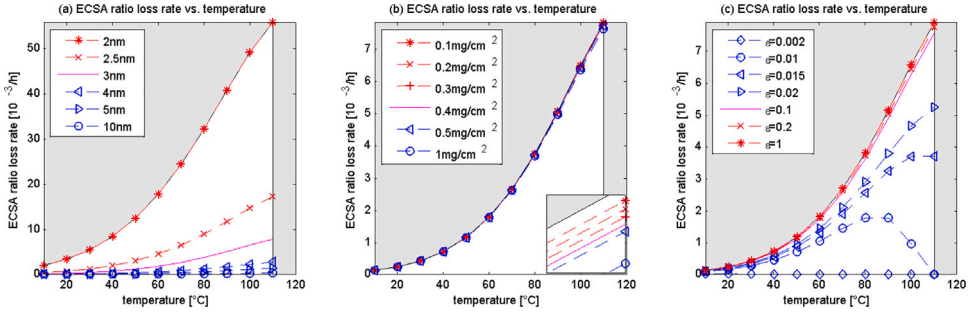

Fig. 4. ECSA ratio loss rate $\dot{E}$ depending on temperature T for various Pt particle diameter d_{Pt} (a), Pt loading p_{Pt} (b), and Pt/C volume fraction ε.

pH in the plot (a) and, conversely, when increasing pH at the selected values of T in the plot (b). We can observe the monotone decrease at all temperatures in (b) and both: the monotone increase al low pH < 1, as well as non-monotone behavior at high pH ≥ 1 in (a).

After reaching some critical values, we found that the theoretical model leaves physical consistency for its variables as stated in (15)–(17). Namely, at some times t the platinum oxide coverage ratio $\theta(t,x)$ becomes fully zero along the whole catalyst thickness $x \in (0,1)$. At $\theta \equiv 0$, no Pt particles remain on the carbon surface, hence the catalyst layer does not work anymore. Therefore, we qualify such states as unfeasible, and we exclude the corresponding critical values from a feasible region for the parameters. For the variable temperature T and pH depicted in Fig. 3, we fill with gray color the unfeasible region, where its complement in white implies the feasible region. The interface between them is formed by the natural restriction pH ≥ 0 in the plot (a), and by the above mentioned inconsistent state $\theta \equiv 0$, if reached at T_{cr} or $\mathrm{pH}_{\mathrm{cr}}$ shown in the plots (a) and (b). Even more interesting is to observe in the plot (c) interplay between the critical values $T_{\mathrm{cr}}(\mathrm{pH})$ and $\mathrm{pH}_{\mathrm{cr}}(\mathrm{T})$ when varying the two parameters T and pH simultaneously.

The analysis of the ECSA ratio loss rate $\dot{E}$ depending on temperature T is presented in Fig. 4 at the selected values of three model parameters of the Pt particle diameter d_{Pt} varying between 2 nm and 10 nm, Pt loading p_{Pt} between 0.1 mg/cm^2 and 1 mg/cm^2, Pt to Carbon volume fraction ε between 0.002 and 1, which are depicted in the plots (a), (b), and (c), respectively. Since the curve in the plot (b) are visually indistinguishable, on the lower right corner we present here a zoom in the small window. We note also a non-monotone behavior of the curves in the plot (c) at low $\varepsilon \leq 0.01$, in contrast to the monotone increase of all other temperature dependencies. Correlations for ionic and electrical conductivities at low volume fraction of conductive phases, together with experimental data are reported in Sánchez-Ramos et al. [46]. The feasible region is bounded by the natural conditions $p_{\mathrm{Pt}} \geq 0$ in (b) and $\varepsilon \leq 1$ in (c), as well as $T \leq T_{\mathrm{cr}}$ with the critical temperature $T_{\mathrm{cr}} = 110$ °C in (a)–(c), and $d_{\mathrm{Pt}} \geq (d_{\mathrm{Pt}})_{\mathrm{cr}}$ in (a) with the critical Pt particle diameter $(d_{\mathrm{Pt}})_{\mathrm{cr}} = 2$ nm, when the inconsistent state $\theta \equiv 0$ is attained.

From Fig. 3(a), (c) and Fig. 4 we summarize our findings with respect to the Temperature Operating Condition:

- The upper threshold for feasible temperature is around 110 °C.
- ECSA ratio loss rate $\dot{E}$ raises when increasing the temperature within 10–110 °C; when increasing Pt/C volume fraction 0.015–1; when decreasing pH in the range 0–0.8, or Pt particle diameter 2–10 nm, or Pt loading 0–1 mg/cm^2.

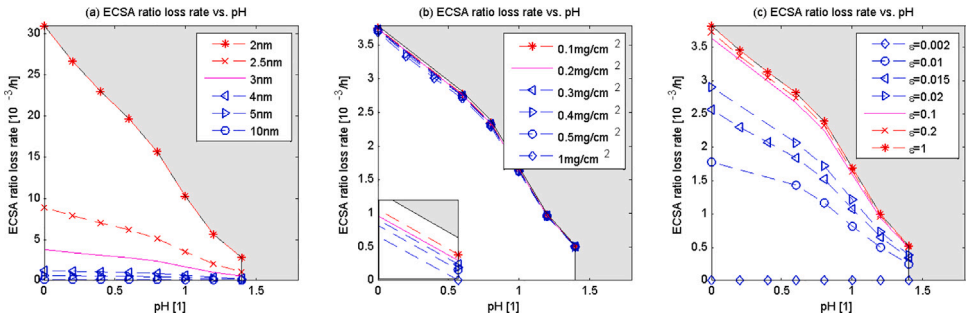

Fig. 5. ECSA ratio loss rate $\dot{E}$ depending on pH for various Pt particle diameter d_{Pt} (a), Pt loading p_{Pt} (b), and Pt/C volume fraction ε (c).

- $\dot{E}$ may drop with increase in the temperature for small Pt/C volume fraction $\varepsilon \le 0.01$, or large pH ≥ 1.
- The impact of Pt particle loading p_{Pt} compared to temperature is nonessential.
- The feasible domain of pH–T parameters is approximated by the following empirical relation between the critical values:

$$pH_{\mathrm{cr}} = \begin{cases} \infty & \text{for } T_{\mathrm{cr}} < 20\ ^\circ\mathrm{C} \\ 0.8 + \dfrac{110 - T_{\mathrm{cr}}}{50} & \text{for } 20\ ^\circ\mathrm{C} \le T_{\mathrm{cr}} \le 110\ ^\circ\mathrm{C} \end{cases} \tag{22}$$

3.2. Sensitivity to pH operating condition

Perfluorosulfonic acid (PFSA) such as the brand named Nafion is the most commonly used ion conducting polymer in the membrane and electrodes, see Meyers [47]. The conducted ion is a proton, and the environment is strongly acidic, which is measured in the non-negative scale of potential of Hydrogen (pH), acidity pH values between 0 and 2 are realistic, see Sethuraman et al. [48]. A higher acidity is corresponding to lower amount of water, thus affecting the membrane and ionomer conductivity. Kneer and Wagner [49] observed that decrease in the wetting state of the catalyst layer results in less platinum catalyst degradation attributed to a lower mobility of dissolved Pt ions at low water content. In the Cyclic Voltammetry (CV) by Bi et al. [31], the Square-Wave (SW) between 0.87 and 1.2 V potentials was applied for 30 s at each potential during 60 operating hours (3,600 cycles). During 5 operating hours (300 potential cycles), significant initial rate $\dot{E}$ about 2.4% per hour was measured.

Overall, platinum dissolution is a process that is closely related to the formation and reduction of Pt oxides. Increased surface oxide coverage of Pt nanoparticle generally reduces the ORR activity of the catalyst by blocking oxygen molecule adsorption, thus slowing down platinum dissolution and degradation process.

From our simulation tests, in Fig. 5 we present the curves of ECSA ratio loss rate $\dot{E}$ in dependence on pH raising from 0 to 1.8. By this, in (a) we plot the several curves for selected Pt particle diameters d_{Pt} from 2 nm to 10 nm, in (b) for Pt loading p_{Pt} from 0.1 mg/cm^2 to 1 mg/cm^2, in (c) for Pt/C volume fractions ε from 0.002 to maximum 1. To distinguish visually the curve in the plot (b) we present on the lower left corner a zoom in the small window. The interface between the feasible region (in white) and unfeasible region (in gray) is presented here, first, by the constraint pH $\le$ pH$_{\mathrm{cr}}$ with the critical pH$_{\mathrm{cr}}$ = 1.4 obtained from the inconsistent state $\theta \equiv 0$, as well as $d_{\mathrm{Pt}} \ge (d_{\mathrm{Pt}})_{\mathrm{cr}}$ with the critical $(d_{\mathrm{Pt}})_{\mathrm{cr}} = 2$ nm in the plot (a). Second, the feasible region corresponds to conditions $p_{\mathrm{Pt}} \ge 0$ in the plot (b), and to $\varepsilon \le 1$ in the plot (c).

From Fig. 3(b) and Fig. 5 we characterize the pH Operating Condition:

- For $T = 80\ ^\circ$C fixed, the upper threshold for feasible pH is around 1.4.
- ECSA ratio loss rate $\dot{E}$ drops when increasing the pH witin 0–1.4; when decreasing temperature 40–110 °C, or Pt/C volume fraction 0.002–1; when increasing Pt particle diameter 2–10 nm, or Pt loading 0–1 mg/cm^2.
- The impact of Pt particle loading p_{Pt} compared to pH is nonessential.

3.3. Sensitivity to Pt particle diameter model parameter

Platinum dissolution and re-deposition are strongly influenced by the particle size distribution (PSD), which represents the number of Pt particles of a given diameter on the carbon support. Dissolution rate is faster for PSD with smaller size, since small particles are thermodynamically less stable then those with larger size. Indeed, the Gibbs–Thomson equation according to Holby et al. [50]

$$E_{\mathrm{GT}}(d,\theta) = \frac{4\Omega\gamma_{\mathrm{total}}}{d} \tag{23}$$

enters as a shift in the Pt ion dissolution reaction rate in (8). The energy E_{GT} and the Pt particle size d are in inverse proportion in (23). Then decreasing d follows increase in the Gibbs–Thomson energy, which matches an increase versus bulk in the dissolution rate.

Materials that catalyze the electrochemical reactions commonly use Pt nanoparticles of 3–5 nm in diameter deposited on carbon blacks, aimed to maximize the electrochemical reaction surface area per platinum amount employed. Smaller 2 nm particles coarsen and lose ECSA rather quickly during aging protocols. The experimental results by Holby et al. [50] demonstrated that ECSA loss rate drops significantly for mean sizes changing from 2–3 nm to 4–5 nm, and almost eliminated for the larger particle sizes. In the study by Sandbeck et al. [51], the Pt particle diameter was varied in the larger range from 2 to 10 nm and reported a continuous decrease in mass activity, that is ECSA, with increasing particle size. However, large particle size distributions may promote catalyst degradation via Ostwald ripening.

In Fig. 6 the numerically computed curves of ECSA ratio loss rate $\dot{E}$ are presented in dependence on the Pt particle diameter d_{Pt} when increasing from 2 nm to 5 nm. We plot the selected $\dot{E}$–d_{Pt} curves for temperatures T varying from 20 °C to 110 °C in the plot (a), for pH from 0 to 1.6 in the plot (b), and for Pt/C volume fractions ε from 0.005 to 1 in the plot (c). In all plots we observe a monotone behavior. When varying the Pt loading, the curves are visually undistinguishable and not presented here. The interface between the feasible and unfeasible, respectively white and gray, regions is determined from the critical temperature T_{cr} =110 °C in (a), from conditions pH $\ge$ 0 in (b), and $\varepsilon \le 1$ in (c).

Based on our numerical experiments reflected in Fig. 6 we describe the Pt Particle Diameter Model Parameter:

- The lower threshold for feasible Pt particle diameter d_{Pt} is 2 nm.
- ECSA ratio loss rate $\dot{E}$ monotonically decreases when increasing the Pt particle diameter d_{Pt} tested witin 2–10 nm; when decreasing temperature 20–110 °C, or Pt/C volume fraction 0.005–1; when increasing pH 0–2, or Pt loading 0–1 mg/cm^2.
- The impact of Pt particle loading p_{Pt} compared to particle diameter is nonessential.

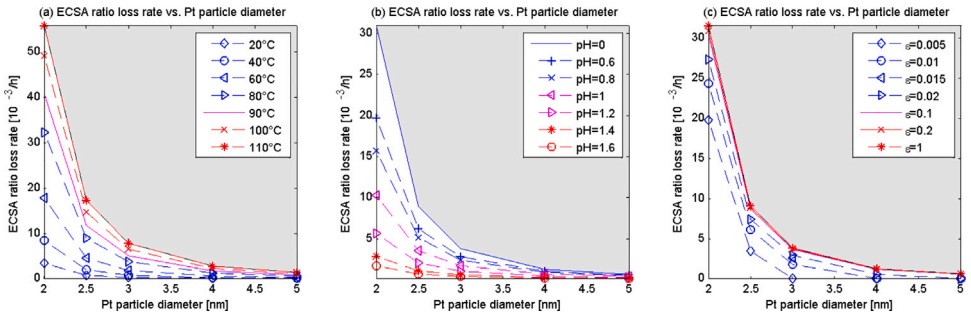

Fig. 6. ECSA ratio loss rate $\dot{E}$ depending on Pt particle diameter d_{Pt} for various temperature T (a), pH (b), and Pt/C volume fraction ε (c).

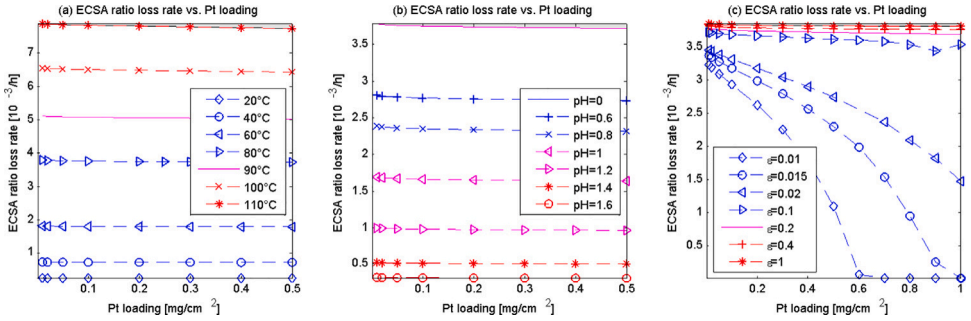

Fig. 7. ECSA ratio loss rate $\dot{E}$ depending on Pt particle loading p_{Pt} for various temperature T (a), pH (b), and Pt/C volume fraction ε (c).

3.4. Sensitivity to Pt particle loading model parameter

In the experiments by Harzer et al. [52], a faster decay of the electrochemical surface area at the Begin of Test (BoT) was observed for low-loaded catalyst layers (0.1 mg/cm^2) compared to those with a higher loading (0.4 mg/cm^2). Comparing different aging protocols, the ECSA loss was more significant for MEA subjected to SW compared to TW modulation. In Gazdzicki et al. [53] it was found, that the cell performance drops significantly at the cathodic Pt loading with a threshold value 0.2–0.3 mg/cm^2.

The experiments subjected to an accelerated stress test according to the U.S. Department of Energy (DOE) recommended square voltage protocol were published recently by Schneider et al. [54]. They report that a higher relative loss in electrochemically active surface area is measured for lower Pt loadings varying between 0.1 and 0.41 mg/cm^2 regardless of the Pt/C ratio and layer thickness. A linear trend between the Pt loading and achieved ECSA is noted at BoT, as expected. Since diffusion depends mainly on the distance to the membrane interface, the Pt loss is stronger at the CL–PEM interface. The ECSA relative loss rate $\{5.2, 4.8, 4.5, 4.3\}$% per hour was mentioned during 4.1(6) operating hours (2500 cycles) when increasing Pt loading $\{0.1, 0.2, 0.32, 0.41\}$ mg/cm^2. This is likely due to the higher thermodynamic stability of larger Pt nanoparticle against dissolution.

From our tests, in Fig. 7 we plot the of ECSA ratio loss rate $\dot{E}$ computed in dependence on the Pt particle loading p_{Pt} when increased from 0 to either 0.5 or 1 mg/cm^2. The curves are selected for plotting under various temperatures T between 20 °C and 110 °C in the plot (a), pH between 0 and 1.6 in the plot (b), and Pt/C volume fractions ε between 0.01 to 1 in the plot (c). We can observe in the plots (a) and (b) very flat curves close to constant, and a similar picture will appear when we vary the Pt particle diameter d_{Pt}. This is refereed to the before mentioned fact that variation in p_{Pt} is nonessential in comparison with variation in T, pH, and d_{Pt}. Whereas the dependence of $\dot{E}$–p_{Pt} curves on Pt/C volume fraction ε in the plot (c) is much more significant. Here we have found only one non-monotone state at $\varepsilon = 0.1$ when decreasing with the Pt loading $\dot{E}$ raises by increase of $p_{\mathrm{Pt}} = 0.9$ mg/cm^2 to $p_{\mathrm{Pt}} = 1$ mg/cm^2.

According to Fig. 7 we qualify the Pt Particle Loading Model Parameter:

- The Pt particle loading p_{Pt} is feasible for all values between 0 and 1 mg/cm^2 tested.
- ECSA ratio loss rate $\dot{E}$ decreases when increasing the Pt particle loading within 0–0.9 mg/cm^2; when decreasing the temperature 20–110 °C, or Pt/C volume fraction 0.01–1; when increasing pH 0–2, or Pt particle diameter 2–10 nm.
- Only the impact on $\dot{E}$ of Pt particle loading p_{Pt} and small Pt/C volume fraction $\varepsilon < 0.1$ is comparative.

3.5. Sensitivity of Pt to carbon volume fraction model parameter

Pt nanoparticles are commonly more homogeneously dispersed on the carbon support at low Pt/C ratio. This leads to a lower degree of Pt agglomeration, hence a lower average particle size and higher ECSA. Ramaswamy et al. [55] showed that a higher volume fraction of ionomer effectively decreases electrode porosity, thus increasing local oxygen transport resistance and tendency to agglomerate (or, equivalently, reduce amount of interior Pt).

Our numerical tests of the of ECSA ratio loss rate $\dot{E}$ in dependence on the Pt/C volume fraction ε when increased from 0.005 to 0.4 are depicted in Fig. 8. For larger values of ε between 0.4 and 1 the curves remain close to constant. In the plot (a) we depict the curves $\dot{E}$–ε at temperature T lying between 20 °C and 110 °C, in the plot (b) at pH between 0 and 1.6, and in the plot (c) at the Pt particle loading p_{Pt} between 0.01 and 1 mg/cm^2. In the small window on the lower right corner in (c) we give a zoom of the closely located curves. The variation in ε is nonessential in comparison with the variation in d_{Pt}, therefore, the Pt particle diameter is not presented here. The interface between the white and gray colored feasible and unfeasible regions is determined by the critical temperature $T_{\mathrm{cr}} = 110$ °C in the plot (a), by the minimum pH = 0 in (b), and minimum $p_{\mathrm{Pt}} = 0$ in (c).

From Fig. 8 we formulate our findings of the Pt/C Volume Fraction Model Parameter:

- The lower threshold for feasible Pt/C volume fraction ε is around 0.005.

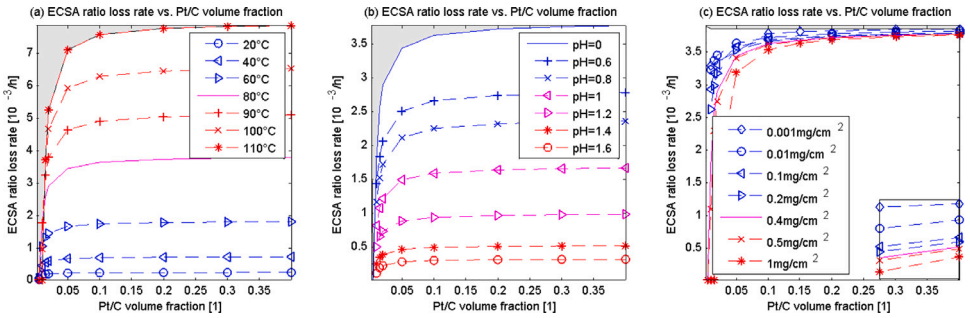

Fig. 8. ECSA ratio loss rate $\dot{E}$ depending on Pt/C volume fraction for various temperature T (a), pH (b), and Pt particle loading p_{Pt} (c).

- ECSA ratio loss rate $\dot{E}$ monotonically increases when increasing the Pt/C volume fraction 0.005–1; when increasing temperature 20–110 °C; when decreasing pH 0–2, or Pt particle diameter d_{Pt} within 2–10 nm, or Pt loading 0–1 mg/cm^2.
- The only variation of small Pt/C volume fraction ε from 0.005 to 0.2 is distinguishable, variation of large ε in the range 0.2–1 has not essential impact on $\dot{E}$.

4. Conclusion

Our modeling of the behavior and maximum allowed range of parameters is based on multi-parametric sensitivity analysis with respect to the ECSA ratio loss rate. It is consistent with the previous theoretical and experimental studies of catalyst degradation and presents new issues characterizing critical values and multiple dependencies. As a result, the feasible PEMFC operating region is mapped correlating the platinum degradation rate with operating conditions and model parameters. The temperature, pH, Pt particle diameter, loading, and Pt/C volume fraction are tested in numerical simulations. This provides helpful hints for designers and engineers to optimize the available setup for achievement of a targeted catalyst lifetime or performance.

Declaration of competing interest

The authors declare that they have no known competing financial interests or personal relationships that could have appeared to influence the work reported in this paper.

Acknowledgments

The author acknowledges the financial support by the University of Graz, Austria.

References

[1] Ball M, Basile A, Veziroğlu T. Compendium of hydrogen energy: hydrogen use, safety and the hydrogen economy. Sawston: Woodhead Publishing; 2016.
[2] Barbir F, Basile A, Veziroğlu T. Compendium of hydrogen energy: hydrogen energy conversion. Sawston: Woodhead Publishing; 2016.
[3] Basile A, Gupta R, Veziroğlu T. Compendium of hydrogen energy: hydrogen storage, distribution and infrastructure. Sawston: Woodhead Publishing; 2016.
[4] Subramani V, Basile A, Veziroğlu T. Compendium of hydrogen energy: hydrogen production and purification. Sawston: Woodhead Publishing; 2015.
[5] Medvedev DA. Trends in research and development of protonic ceramic electrolysis cells. Int J Hydrog Energy 2019;44(49):26711–40. http://dx.doi.org/10.1016/j.ijhydene.2019.08.130.
[6] Evangelisti S, Tagliaferri C, Brett D, Lettieri P. Life cycle assessment of a polymer electrolyte membrane fuel cell system for passenger vehicles. J Clean Prod 2017;142(4):4339–55. http://dx.doi.org/10.1016/j.jclepro.2016.11.159.
[7] Ferrara A, Jakubek S, Hametner C. Energy management of heavy-duty fuel cell vehicles in real-world driving scenarios: Robust design of strategies to maximize the hydrogen economy and system lifetime. Energy Convers Manag 2021;232:113795. http://dx.doi.org/10.1016/j.enconman.2020.113795.
[8] Gallo M, Marinelli M. The impact of fuel cell electric freight vehicles on fuel consumption and CO2 emissions: The case of Italy. Sustainability 2022;14(20):13455. http://dx.doi.org/10.3390/su142013455.
[9] Petrone R, Hissel D, Péra M, Chamagne D, Gouriveau R. Accelerated stress test procedures for PEM fuel cells under actual load constraints: State-of-art and proposals. Int J Hydrog Energy 2015;40(36):12489–505. http://dx.doi.org/10.1016/j.ijhydene.2015.07.026.
[10] Macauley N, Papadias D, Fairweather J, Spernjak D, Langlois D, Ahluwalia R, et al. Carbon corrosion in PEM fuel cells and the development of accelerated stress tests. J Electrochem Soc 2018;165(6):F3148–60. http://dx.doi.org/10.1149/2.0061806jes.
[11] Stropnik R, Mlakar N, Lotrič A, Sekavčnik M, Mori M. The influence of degradation effects in proton exchange membrane fuel cells on life cycle assessment modelling and environmental impact indicators. Int J Hydrog Energy 2022;47(57):24223–41. http://dx.doi.org/10.1016/j.ijhydene.2022.04.011.
[12] Eikerling M, Kulikovsky A. Polymer electrolyte fuel cells. Amsterdam: Elsevier; 2017.
[13] Kulikovsky AA. Analytical modeling of fuel cells. Amsterdam: Elsevier; 2019, http://dx.doi.org/10.1016/C2018-0-01182-2.
[14] Hacker V, Mitsushima S. Fuel cells and hydrogen. Amsterdam: Elsevier; 2018.
[15] Bazant MZ. Theory of chemical kinetics and charge transfer based on nonequilibrium thermodynamics. Acc Chem Res 2013;46(5):1144–60. http://dx.doi.org/10.1021/ar300145c.
[16] Fellner K, Kovtunenko V. A discontinuous Poisson–Boltzmann equation with interfacial transfer: homogenisation and residual error estimate. Appl Anal 2016;95(12):2661–82. http://dx.doi.org/10.1080/00036811.2015.1105962.
[17] González-Granada J, Kovtunenko V. Entropy method for generalized Poisson–Nernst–Planck equations. Anal Math Phys 2018;8(4):603–19. http://dx.doi.org/10.1007/s13324-018-0257-1.
[18] Kovtunenko V, Zubkova A. Mathematical modeling of a discontinuous solution of the generalized Poisson–Nernst–Planck problem in a two-phase medium. Kinet Relat Mod 2018;11(1):119–35. http://dx.doi.org/10.3934/krm.2018007.
[19] Khludnev A, Kovtunenko V. Analysis of cracks in solids. Int. ser. adv. fract. mech., vol. 6, Southampton, Boston: WIT-Press; 2000.
[20] Kovtunenko VA. Quasi-variational inequality for the nonlinear indentation problem: a power-law hardening model. Phil Trans R Soc A 2022;380(2236):20210362. http://dx.doi.org/10.1098/rsta.2021.0362.
[21] Karpenko-Jereb L, Sternig C, Fink C, Tatschl R. Membrane degradation model for 3D CFD analysis of fuel cell performance as a function of time. Int J Hydrog Energy 2016;41(31):13644–56. http://dx.doi.org/10.1016/j.ijhydene.2016.05.229.
[22] Kulikovsky AA. Understanding catalyst layer degradation in PEM fuel cell through polarization curve fitting. Electrocatalysis 2014;5:221–5. http://dx.doi.org/10.1007/s12678-014-0191-4.
[23] Pandy A, Yang Z, Gummalla M, Atrazhev V, Kuzminyh N, Sultanov V, et al. A carbon corrosion model to evaluate the effect of steady state and transient operation of a polymer electrolyte membrane fuel cell. J Electrochem Soc 2013;160(9):F972–9. http://dx.doi.org/10.1149/2.036309jes.
[24] Kravos A, Kregar A, Mayer K, Hacker V, Katrašnik T. Identifiability analysis of degradation model parameters from transient CO_2 release in low-temperature PEM fuel cell under various AST protocols. Energies 2021;14(14):4380. http://dx.doi.org/10.3390/en14144380.
[25] Frühwirt P, Kregar A, Törring J, Katrašnik T, Gescheidt G. Holistic approach to chemical degradation of Nafion membranes in fuel cells: modelling and predictions. Phys Chem Chem Phys 2020;22(10):5647–66. http://dx.doi.org/10.1039/C9CP04986J.
[26] Cherevko S, Kulyk N, Mayrhofer K. Durability of platinum-based fuel cell electrocatalysts: Dissolution of bulk and nanoscale platinum. Nano Energy 2016;29(10):275–98. http://dx.doi.org/10.1088/0957-4484/21/2/025701.
[27] Holby E, Morgan D. Application of Pt nanoparticle dissolution and oxidation modeling to understanding degradation in PEM fuel cells. J Electrochem Soc 2012;159(5):B578–91. http://dx.doi.org/10.1149/2.011204jes.
[28] Darling R, Meyers J. Kinetic model of platinum dissolution in PEMFCs. J Electrochem Soc 2003;150(11):A1523–7. http://dx.doi.org/10.1149/1.1613669.

[29] Li Y, Moriyama K, Gu W, Arisetty S, Wang C. A one-dimensional Pt degradation model for polymer electrolyte fuel cells. J Electrochem Soc 2015;162(8):F834–42. http://dx.doi.org/10.1149/2.0101508jes.
[30] Zheng Z, Yang F, Lin C, Zhu F, Shen S, Wei G, et al. Design of gradient cathode catalyst layer (CCL) structure for mitigating Pt degradation in proton exchange membrane fuel cells (PEMFCs) using mathematical method. J Power Sources 2020;451:227729. http://dx.doi.org/10.1016/j.jpowsour.2020.227729.
[31] Bi W, Sun Q, Deng Y, Fuller T. The effect of humidity and oxygen partial pressure on degradation of Pt/C catalyst in PEM fuel cell. Electrochim Acta 2009;54(6):1826–33. http://dx.doi.org/10.1016/j.electacta.2008.10.008.
[32] Jahnke T, Futter G, Baricci A, Rabissi C, Casalegno A. Physical modeling of catalyst degradation in low temperature fuel cells: Platinum oxidation, dissolution, particle growth and platinum band formation. J Electrochem Soc 2020;167:013523. http://dx.doi.org/10.1149/2.0232001JES.
[33] Kregar A, Gatalo M, Maselj N, Hodnik N, Katrašnik T. Temperature dependent model of carbon supported platinum fuel cell catalyst degradation. J Power Sources 2021;514:230542. http://dx.doi.org/10.1016/j.jpowsour.2021.230542.
[34] Tomić A, Pivac I, Barbir F. A review of testing procedures for proton exchange membrane electrolyzer degradation. J Power Sources 2023;557:232569. http://dx.doi.org/10.1016/j.jpowsour.2022.232569.
[35] Ritzberger D, Höflinger J, Du Z, Hametner C, Jakubek S. Data-driven parameterization of polymer electrolyte membrane fuel cell models via simultaneous local linear structured state space identification. Int J Hydrog Energy 2021;46(21):11878–93. http://dx.doi.org/10.1016/j.ijhydene.2021.01.037.
[36] Correa J, Farret F, Popov V, Simões M. Sensitivity analysis of the modeling parameters used in simulation of proton exchange membrane fuel cells. IEEE Trans Energy Convers 2005;20(1):211–8. http://dx.doi.org/10.1109/TEC.2004.842382.
[37] Min C, He Y, Liu X, Yin B, Jiang W, Tao W. Parameter sensitivity examination and discussion of PEM fuel cell simulation model validation: Part II: Results of sensitivity analysis and validation of the model. J Power Sources 2006;160(1):374–85. http://dx.doi.org/10.1016/j.jpowsour.2006.01.080.
[38] Pant L, Stewart S, Craig N, Weber A. Critical parameter identification of fuel-cell models using sensitivity analysis. J Electrochem Soc 2021;168(7):074501. http://dx.doi.org/10.1149/1945-7111/ac0d68.
[39] Kovtunenko V, Karpenko-Jereb L. Study of voltage cycling conditions on Pt oxidation and dissolution in polymer electrolyte fuel cells. J Power Sources 2021;493:229693. http://dx.doi.org/10.1016/j.jpowsour.2021.229693.
[40] Euro harmonised test protocols for PEMFCs in hydrogen vehicles. Fuel Cells Bull 2016;2016(4):9–10. http://dx.doi.org/10.1016/S1464-2859(16)30088-8.
[41] Karpenko-Jereb L, Kovtunenko V. Modeling of the impact of cycling operating conditions on durability of polymer electrolyte fuel cells and its sensitivity analysis. Int J Hydrog Energy 2023;48(41):15646–56. http://dx.doi.org/10.1016/j.ijhydene.2023.01.029.
[42] Pivac I, Barbir F. Impact of shutdown procedures on recovery phenomena of proton exchange membrane fuel cells. Fuel Cells 2020;160(2):185–95. http://dx.doi.org/10.1002/fuce.201900174.
[43] Kregar A, Kravos A, Katrašnik T. Methodology for evaluation of contributions of Ostwald ripening and particle agglomeration to growth of catalyst particles in PEM fuel cells. Fuel Cells 2020;20(4):487–98. http://dx.doi.org/10.1002/fuce.201900208.
[44] Zhao N, Chu Y, Xie Z, Eggen K, Girard F, Shi Z. Effects of fuel cell operating conditions on proton exchange membrane durability at open-circuit voltage. Fuel Cells 2020;20(2):176–84. http://dx.doi.org/10.1002/fuce.201900173.
[45] Maselj N, Gatalo M, Ruiz-Zepeda F, Kregar A, Jovanovič P, Hodnik N, et al. The importance of temperature and potential window in stability evaluation of supported Pt-based oxygen reduction reaction electrocatalysts in thin film rotating disc electrode setup. J Electrochem Soc 2020;167(11):114506. http://dx.doi.org/10.1149/1945-7111/aba4e6.
[46] Sánchez-Ramos A, Gostick J, García-Salaberri P. Modeling the effect of low Pt loading cathode catalyst layer in polymer electrolyte fuel cells: Part I. Model formulation and validation. J Electrochem Soc 2021;168(12):124514. http://dx.doi.org/10.1149/1945-7111/ac4456.
[47] Meyers RA. Encyclopedia of sustainability science and technology. New York: Springer; 2020, http://dx.doi.org/10.1007/978-1-4939-2493-6.
[48] Sethuraman V, Weidner J, Haug A, Motupally S, Protsailo L. Hydrogen peroxide formation rates in a PEMFC anode and cathode: effect of humidity and temperature. J Electrochem Soc 2007;155(1):B50–7. http://dx.doi.org/10.1149/1.28019800.
[49] Kneer A, Wagner N. A semi-empirical catalyst degradation model based on voltage cycling under automotive operating conditions in PEM fuel cells. J Electrochem Soc 2019;166(2):F120–7. http://dx.doi.org/10.1149/2.0641902jes.
[50] Holby E, Sheng W, Shao-Horn Y, Morgan D. Pt nanoparticle stability in PEM fuel cells: influence of particle size distribution and crossover hydrogen. Energy Environ Sci 2009;2(8):865–71. http://dx.doi.org/10.1039/B821622N.
[51] Sandbeck D, Secher N, Speck F, Sørensen J, Chorkendorff J, Cherevko S. Particle size effect on platinum dissolution: considerations for accelerated stability testing of fuel cell catalysts. ACS Catal 2020;10(11):6281–90. http://dx.doi.org/10.1021/acscatal.0c00779.
[52] Harzer G, Schwämmlein J, Damjanović A, Ghosh S, Gasteiger H. Cathode loading impact on voltage cycling induced PEMFC degradation: A voltage loss analysis. J Electrochem Soc 2018;165(6):F3118–32. http://dx.doi.org/10.1149/2.0161806jes.
[53] Gazdzicki P, Mitzel J, Dreizler AM, Schulze M, Friedrich K. Impact of platinum loading on performance and degradation of polymer electrolyte fuel cell electrodes studied in a rainbow stack. Fuel Cells 2017;18(3):270–8. http://dx.doi.org/10.1002/fuce.201700099.
[54] Schneider P, Batool M, Godoy A, Singh R, Gerteisen D, Jankovic J, et al. Impact of platinum loading and layer thickness on cathode catalyst degradation in PEM fuel cells. J Electrochem Soc 2023;170(2):024506. http://dx.doi.org/10.1149/1945-7111/acb8df.
[55] Ramaswamy N, Kumaraguru S, Gu W, Kukreja R, Yu K, Groom D, et al. High-current density durability of Pt/C and PtCo/C catalysts at similar particle sizes in PEMFCs. J Electrochem Soc 2021;168(2):024519. http://dx.doi.org/10.1149/1945-7111/abe5ea.